Impact of surface enrichment and morphology on sputtering of EUROFER by deuterium

R. Arredondo[a)]*, M. Balden[a)], A. Mutzke[b)], U. von Toussaint[a)], S. Elgeti[a)], T. Höschen[a)], K. Schlueter[a)], M. Mayer[a)], M. Oberkofler[a)], W. Jacob[a)]

a) Max-Planck-Institut für Plasmaphysik, Boltzmannstr. 2, D-85748 Garching, Germany
b) Max-Planck-Institut für Plasmaphysik, Wendelsteinstrasse 1, D-17491 Greifswald, Germany

*rodrigo.arredondo@ipp.mpg.de

Abstract

EUROFER is a Reduced Activation Ferritic Martensitic (RAFM) steel developed as structural material for future fusion power plants and is considered as first-wall material in recessed areas of DEMO. Recent work has shown a fluence-dependent decrease of the sputter yield for bombardment with deuterium ions in the energy range of 100 to about 500 eV. This decrease was previously attributed to preferential sputtering of the lower mass constituents in EUROFER, such as Fe and Cr, compared to the higher mass alloying elements. This leads to an increase of the surface tungsten concentration. However, it was also observed that, after sputtering, the samples had developed a very rough surface morphology. In this work, the combined influence of surface roughness and W surface enrichment on the sputter yield of EUROFER under bombardment with 200 eV deuterium ions was studied. The influence of surface roughness was determined with the aid of Scanning Electron Microscopy (SEM) and SDTrimSP-3D simulations. W surface enrichment was investigated applying sputter X-Ray Photoelectron Spectroscopy (XPS) depth-profiling and Rutherford backscattering spectrometry (RBS). After bombardment to a fluence of 10^{24} D m^{-2} (at 200 eV per deuterium) a reduction of the sputter yield to 29 % ± 5 % of the initial value was measured by weight-loss measurements. This reduction is in good agreement with published values. Two distinct surface morphologies, consisting of smooth and spiked surfaces, were observed on the EUROFER sample after sputtering. Based on the experimental results, the combined effect of the two factors, surface roughness and W surface enrichment, is estimated to be responsible for a reduction in the sputter yield to 27 % ± 4 % of the initial value, which is in excellent agreement with the measured value. Our assessment shows that both surface morphology and W surface enrichment contribute significantly to the reduction of the sputter yield of EUROFER under the given experimental conditions, and are sufficient to fully explain the experimentally observed reduction in the sputter yield.

Keywords: Sputtering, EUROFER, RAFM, SDTrimSP, Roughness, SDTrimSP-3D, SEM, Sputter-XPS

1 Introduction

EUROFER is a Reduced Activation Ferritic Martensitic (RAFM) steel developed by the European Union fusion materials community as structural material for use in fusion applications [1,2]. It is optimized for low neutron activation and good mechanical properties. Additionally, EUROFER displays low H solubility, ease of manufacturing and low cost (compared with W, foreseen as cladding in the first-wall and divertor regions). Similarly to other RAFM steels (e.g., RUSFER [3], F82H [4], CLAM [5]), EUROFER is composed of Fe, Cr (~ 9 at. %), C (~ 0.45 at. %), Mn (~ 0.4 at. %), W (~ 0.33 at. %), V (~ 0.2 at. %), Ta (~ 0.04 at. %) and small amounts of other alloying elements [1]. EUROFER or other RAFM steels are foreseen as structural material in DEMO. Their use is also planned for the breeding-blanket (i.e., first-wall elements) [1], where they would be clad with W to reduce erosion. W cladding is technologically challenging and could prove expensive. Therefore, it would be technically and economically advantageous to eliminate the W cladding in areas where the erosion of pure EUROFER would be sufficiently low, such as parts of the first-wall that have no direct plasma contact. Such areas could still be exposed to a flux of charge-exchange neutral particles with an energy spectrum in the range of almost 0 eV to several keV [6,7]. Consequently, erosion of EUROFER and other RAFM steels due to sputtering must be investigated. The following work focuses exclusively on EUROFER under one specific exposure scenario, and builds upon the work shown in [8].

If EUROFER is bombarded with D, it exhibits W (and, more modestly, Ta) surface enrichment which can be attributed to preferential sputtering [9,10,11], as atoms of Fe or Cr are more easily sputtered than atoms of W or Ta. Additionally, during bombardment EUROFER develops a distinct, heterogeneous surface morphology. The morphology of the surface is dependent on the sample

temperature during exposure, the incident particle energy and the accumulated fluence [9,10,12,13,14,15]. A progressive reduction in the sputter yield (SY) has been confirmed experimentally, which would be consistent with the progressive formation of a surface layer rich in W due to preferential sputtering [9,13,16]. It is worth noting that the impact of the surface morphology of EUROFER on the sputter yield has not yet been investigated.

Monte-Carlo-based codes are available for simulation of sputtering. While simulations with codes such as SDTrimSP [17,18] predict W and Ta surface enrichment, when simulating the exposure, the evolution of the sputter yield of EUROFER does not agree quantitatively with the experimental data [9]. Due to the complex structure and composition of the material, static calculations with SDTrimSP do not provide correct results for deuterium bombardment on EUROFER. Furthermore, since the target composition is very different from a homogeneous one, both in its initial state and during bombardment, even dynamic calculations with the 1-D code are of only limited use. Only the results of the 3-dimensional version of the code, SDTrimSP-3D, show good agreement with the experimental results. With the use of this code, the erosion behavior and evolution of surface structures like the ones observed experimentally can be calculated, as will be shown in Sec. 4.

In this work, it was attempted to disentangle the impact on the sputter yield of D on EUROFER of surface morphology and of W and Ta surface enrichment by studying each effect separately. The EUROFER samples were exposed to a mono-energetic, mass-selected ion beam in the SIESTA device [19]. The surface morphology of EUROFER extracted from Scanning Electron Microscopy (SEM) images was employed to provide a basis for SDTrimSP-3D simulations [20], the 3-D version of the SDTrimSP code [17], which is capable of simulating ion bombardment under arbitrary, complex target geometries. These simulations were used to quantify the effect of the measured surface morphology on the sputter yield. The effect of the W and Ta surface enrichment on the sputter yield was quantified with 1-D SDTrimSP [17] simulations with an enriched layer consistent with sputter X-Ray Photoelectron Spectrometry (XPS) and Rutherford Backscattering Spectrometry (RBS) measurements. The corresponding reduction of the sputter yield due to these two effects is compared with experimental data determined via weight-loss measurements in this work and to data from literature. Additionally, Electron Backscatter Diffraction (EBSD), Energy Dispersive X-ray spectroscopy (EDX) and Confocal Laser Scanning Microscopy (CLSM) were performed in an attempt to identify grain-dependent effects. This study constitutes a first of its kind, as it has hitherto not been attempted to investigate the impact of surface morphology on the sputtering behavior of EUROFER. As such, it focuses on a single exposure scenario and offers limited statistics. Follow-up studies must be performed to further corroborate the findings shown here.

2 Experimental methodology and simulations

EUROFER samples were cut from a plate of EUROFER97-2 (heat 993,393, originally produced in 2005 for Forschungszentrum Karlsruhe, Germany) to a size of 12×15×0.7 mm^3. The samples were polished with OP-U 0.04 µm to a mirror finish and the surface morphology was characterized prior to exposure by SEM and AFM (Atomic Force Microscopy). The samples were determined to be sufficiently smooth, following the criteria discussed in [21], with a root-mean-squared roughness value $R_{RMS} \simeq 2$ nm and a distribution of local slopes lower than 15° at the 95th percentile. FIB (Focused Ion Beam) markers were cut at several points on one sample to enable imaging of the same location before and after exposure. Additionally, FIB-induced Pt-coatings were placed at several locations. These localized coatings protected the underlying area from ion bombardment in SIESTA and allowed the identification of the position of the original surface after erosion. EBSD and EDX were also performed at pre-defined locations, thereby obtaining information on the grain orientation and initial distribution of W on the sample surface. SEM was performed using the SE (Secondary Electron) detector of the Auriga60 from ZEISS, equipped with an EDX detector (Bruker, Esprit, Quantax 400-Z30). In all cases, the electron energy was 5 keV. For the EBSD measurements, a HELIOS NanoLab600 from FEI

was used, equipped with an AZtechHKL Symmetry detector (Oxford Instruments). The tilt angle for the EBSD measurements was 57°. The electron energy was set to 20 keV.

It was previously observed that degassing of the sample due to annealing in vacuum and during exposure in SIESTA could lead to a change in the sample weight, thereby corrupting the weight-loss measurements. To accurately measure the weight-loss only due to erosion, the sample was annealed in SIESTA at roughly 600 K for 3 hours prior to exposure via electron-impact heating on the back of the sample, thereby allowing it to degas. The sample was subsequently exposed to a mono-energetic, mass-filtered 600 eV D_3^+ ion beam (equivalent to 200 eV per deuteron) by applying an accelerating potential of 4.7 kV at the ion source and positively biasing the sample to 4.1 kV. The sample was bombarded under normal incidence to a final fluence of 1.14×10^{24} D m^{-2} in three fluence steps. The temperature of the sample during exposure was approximately 300 K, as measured with a type K thermocouple. The sample with the sample holder was weighed in-situ before and after each exposure. Ex-situ weight measurements were also performed between exposures for comparison with data from literature, where the sputter yield was also determined via ex-situ weight-loss measurements (e.g., [9]). In order to assess the effect of exposing the sample to air between erosion steps at SIESTA, 3 days after the final erosion step, the sample was re-inserted in vacuum in SIESTA and weighed in-situ.

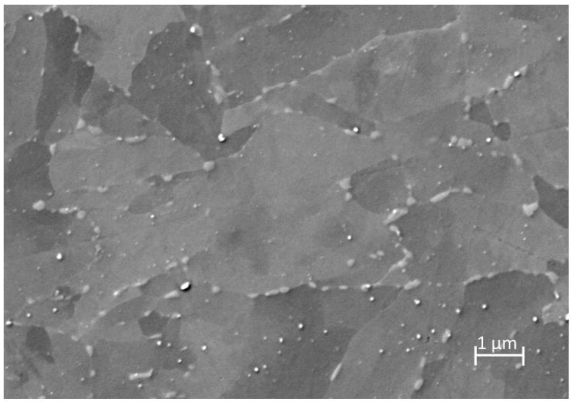

Figure 1 SEM micrograph of a EUROFER sample before exposure in SIESTA. EDX scans of the sample reveal that the small bright areas on the image correspond to segregations, predominantly carbides. These segregations contain a significant amount of Cr, W and Ta, and appear preferentially near grain-boundaries.

The quasi-differential sputter yield was determined by dividing the in- and ex-situ weight-loss measurements by the impinging ion fluence during each exposure step. Therefore, the calculated values correspond to the fluence-dependent sputter yields of EUROFER averaged over their respective fluence steps.

An SEM image of EUROFER before exposure is shown in Fig. 1. After the final exposure, the sample surface was again characterized with SEM, revealing two main types of morphologies: relatively flat, smooth areas much like the surface prior to exposure, and areas with spiked structures, both shown in Fig. 2. The spikes have a typical height, width and spacing of roughly 24 nm, 18 nm and 24 nm, respectively, as measured on tilted SEM images with a measurement uncertainty of ± 2 nm (Fig. 2-b), though these dimensions varied by 5 – 10 nm among the measured spikes. AFM scans were attempted. However, the surface morphology of the spiked structures could not be correctly resolved. Due to the small size of the spikes relative to the AFM scanning tip, the spikes were "smoothed" over the tip radius and the scanning tip could not probe the valleys between spikes. The absolute thickness of the eroded layer was calculated for the spiked morphology with the aid of FIB cross-sections of local Pt-coatings deposited by FIB before the first erosion step. The eroded layer thickness was measured in the FIB-cross section as the height difference between the section protected by the Pt-coating (not eroded) and the neighboring eroded area, which featured the spiked surface morphology. Stereophotogrammetry was applied to SEM images taken normal to the surface and taken at an angle (Fig. 3) to determine the thickness of the eroded layer for the smooth morphology relative to the

spiked morphology. It was determined that the areas with the smooth surface morphology were eroded substantially less than the areas featuring the rough surface morphology. However, the uncertainty in the measurement of the eroded layer thickness by this method was significant (of the order of 10 nm). The eroded layer thickness of the areas featuring a smooth morphology was used to quantify the sputter yield of these areas.

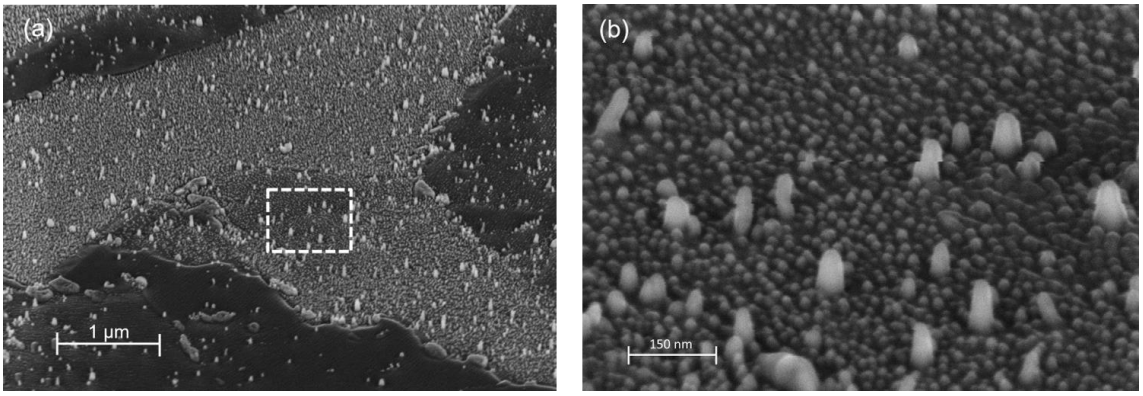

Figure 2 (a): Tilted SEM image of spiked and smooth surface morphologies of EUROFER exposed to a total D fluence of 1.14×10^{24} D m^{-2} at 200 eV/D and 300 K. (b): Close-up of the area inside the dashed white square in the left image. The larger pillars are segregations, mainly carbides.

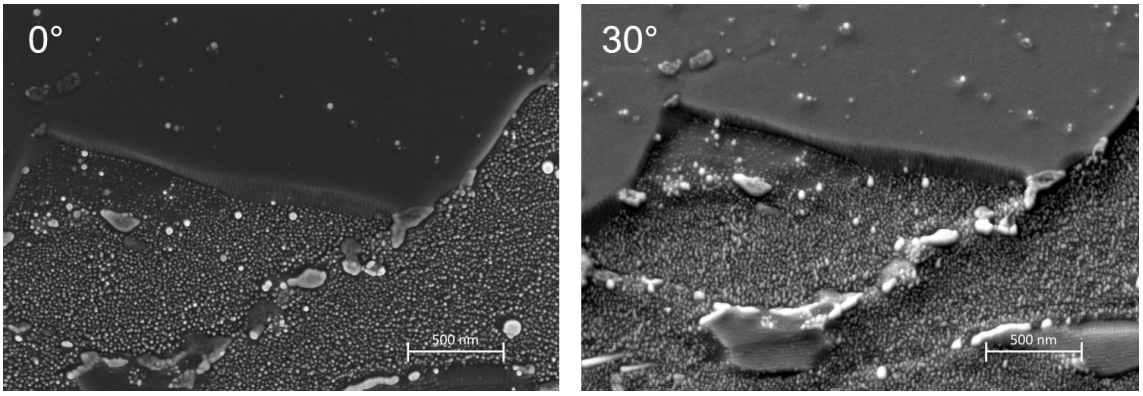

Figure 3 (a) SEM image of spiked and smooth surface morphologies of exposed EUROFER. (b) SEM image of the same area tilted by 30°, indicating via stereophotogrammetry that the smooth surface was eroded roughly 90 nm less than the spiked area. The bright particles correspond to segregations, chiefly in the form of carbides.

With the aid of the FIB markers, EDX was performed on the same locations as prior to exposure in SIESTA, thereby allowing a direct comparison of the W distribution near the surface. Sputter-XPS measurements of the sample were performed post-exposure to quantify the W, Ta and Cr concentration within the first 20 nm of depth. CLSM imaging was employed on the same areas where EBSD was performed to correlate eroded layer thickness for each grain with grain orientation [22].

Static simulations to quantify the effect of the surface morphology on the sputter yield were performed by modelling the sputtering behavior of the smooth surface with SDTrimSP (1-D) and that of the spiked surface with SDTrimSP-3D (shown in Fig. 4). In all simulations, a simplified, homogeneous EUROFER composition was used, consisting of 99.67 at. % Fe and 0.33 at. % W. The 9 at. % of Cr present in EUROFER were neglected (substituted by Fe) because the sputter yields of 200 eV D on Fe and on Cr are very similar [23]. Therefore, their inclusion in this case would not alter the simulated sputtering behavior. The remaining alloying elements were also neglected: due to their small concentrations and/or their comparable sputter yields, their substitution by Fe does not have an impact on the overall sputtering behavior. The overall change in the sputter yield due to the surface morphology was taken as a weighted arithmetic mean of the sputter yields of the flat and spiked surface morphologies observed in the SEM images. The weighting factor was the fraction of the surface area in which each kind of morphology was observed. The weighted mean was divided by the

sputter yield from the 1-D simulation to calculate the degree of reduction of the SY due to surface morphology.

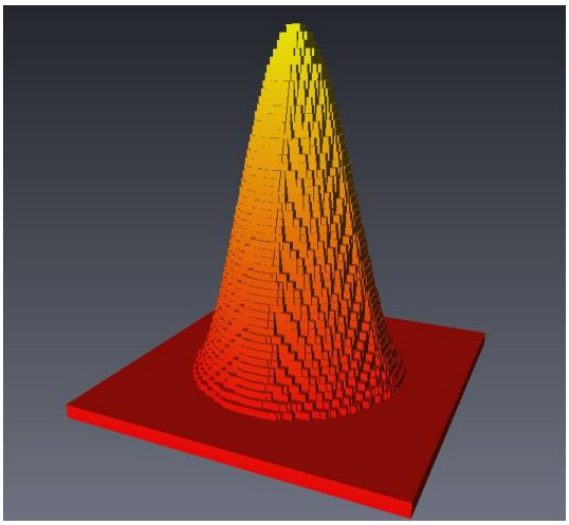

Figure 4 3-D model of spike used in SDTrimSP-3D simulations of EUROFER, consisting of a truncated $\cos^2$ surface with a flat base and periodic boundary conditions on its sides. The height, width and spacing are, respectively, 25 nm, 17.5 nm and 24 nm, based on multiple measurements on tilted SEM images (Fig. 2-b).

To calculate the effect of W and Ta surface enrichments on the sputter yield, sputter-XPS was performed with a PHI 5600 ESCA system equipped with an Al K_α X-ray source. W, Ta and Cr depth profiles were obtained by sputter-erosion using a beam of 10 keV Ar^+ ions at an incident angle of 20° relative to the surface normal, and periodically recording the photoelectron spectra between erosion steps. The analysis area was for all measurements roughly 0.4×0.4 mm^2. The Ar^+ beam with a beam-spot of approximately 150 µm in diameter was scanned over an area of 1.2×1.5 mm^2, creating an evenly sputtered analysis area. Static SDTrimSP simulations were performed with the previously-mentioned bulk composition and with additional surface layers with a W and Ta concentrations consistent with the elemental spectra measured by sputter-XPS, with the aid of a forward-modeling code that estimates the likely XPS spectra for a given depth-dependent sample composition [24]. RBS measurements were performed to verify the results of the forward-modeling code with 1, 1.5 and 2 MeV incident ^4He ions at a scattering angle of 165° using a PIPS (Passivated Implanted Planar Silicon) detector with an energy resolution of 15 keV and a solid angle of 1.11 msr. The analysis area for RBS was 1×1 mm^2. The spectra were evaluated using the program SIMNRA [25].

The sputter yield obtained from these SDTrimSP simulations was divided by that of the previous static SDTrimSP 1-D simulation (99.67 at. % Fe and 0.33 at. % W) to calculate the degree of reduction of the sputter yield, SY, which could be attributed solely to W and Ta enrichment.

The overall reduction of the sputter yield due to the compounded effects of surface morphology and surface enrichment was calculated by multiplying the reduction factor calculated in each individual case. This merged value was compared to the reductions in the sputter yields calculated from the weight-loss measurements and from literature [9].

3 Experimental results and comparison to SDTrimSP-3D

The spiked morphology extracted from the SEM images (Fig. 2) was modelled as a truncated cosine-squared ($\cos^2$) surface with a flat base in SDTrimSP-3D with periodic boundary conditions, as shown in Fig. 4. Compared with a 1-D, static simulation with SDTrimSP for a flat surface, the sputter yield of the simulated surface is reduced by 24 % from 0.036 to 0.028, i.e.,

$$SY_{Rough} = (1 - 0.24) \times SY_{1D\ flat} = 0.76 \times SY_{1D\ flat}.$$

If the sputter yield of EUROFER under the present experimental conditions were $SY_{1D\ flat}$, then the expected eroded layer thickness would be 135 nm. Imaging of a FIB cross-section performed along an exposed area of the sample and an area protected by a FIB-coating indicates that the thickness of the eroded layer was roughly 120 nm for the spiked surface morphology, shown in Fig. 5. In all investigated SEM images the areas with a smooth morphology have suffered less erosion than the areas featuring a spiked surface morphology. Figure 3 shows two SEM images of exposed EUROFER at the same position. One image is normal to the surface while the other is tilted at an angle of 30° to the surface normal. Stereophotogrammetric analysis reveals that for these images the smooth surface is elevated approximately 90 nm – 110 nm above the bottom of the spiked surface. This is confirmed in CLSM images, which also show this height difference within the measurement uncertainty, though the two kinds of surface morphologies cannot be adequately resolved with CLSM due to the limited lateral resolution. Therefore, since the thickness of the eroded layer for the spiked surface was measured as 120 nm, the eroded layer thickness of the smooth surface shown in Fig. 3 is between 10 nm and approximately 30 nm. Within the experimental uncertainty of ± 10 nm, the eroded layer thickness of the smooth surface morphology is between 0 nm (no net erosion, SY = 0) and 40 nm (30% of 135 nm, SY = 30% of $SY_{1D\ flat}$), i.e.,

$$SY_{Smooth} = (0.15 \pm 0.15) \times SY_{1D\ flat}.$$

Figure 6 shows a typical distribution of both kinds of surface morphologies on the exposed EUROFER sample. The fraction of surface area occupied by each kind of morphology was obtained by applying a contrast filter on SEM images of EUROFER after erosion, as it was noted that the secondary electron image was brighter for the spiked surface than for the smooth surface. Abundant segregations are visible in the SEM images (e.g., Fig. 3), corresponding to very light spikes or irregular structures. These are predominantly carbides, as evidenced by EDX. The majority of the exposed area (A = 70 % ± 5 %) is covered by the spiked surface morphology, while the remaining area is mostly flat. Therefore, the sputter yield averaged over the two kinds of surface morphologies is:

$$SY_{Morphology} = A \times SY_{Rough} + (1 - A) \times SY_{Smooth}.$$

This value is:

$$SY_{Morphology} = [(0.7 \pm 0.05) \times 0.76 + \times (0.3 \pm 0.05) \times (0.15 \pm 0.15)] \times SY_{1D\ flat} = (0.58 \pm 0.054) \times SY_{1D\ flat},$$

i.e., a reduction of the sputter yield due to surface morphology of 42 % ± 5 %. The calculation of the uncertainty was performed following the standard rules of uncertainty propagation. It is still unclear why two distinct surface morphologies with different sputtering behaviors emerge in EUROFER bombarded under these conditions. Possible reasons are discussed in Section 4.

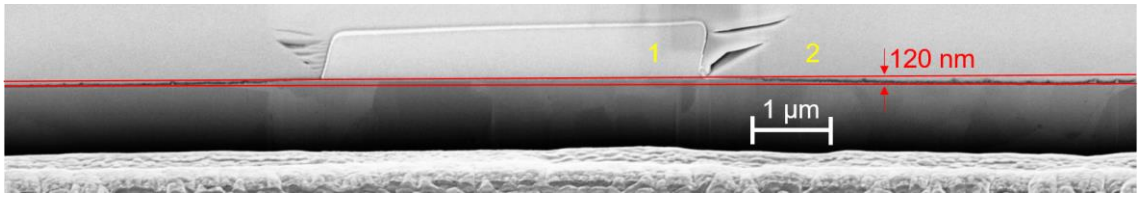

Figure 5 FIB cross-section of exposed EUROFER. The FIB cover layer labeled “1” was deposited before bombardment of the sample in SIESTA, thereby protecting the underlying area from erosion. The cover layer labeled “2” was deposited after exposure for the purpose of the FIB cut and overlaps layer “1”. The thickness of the eroded layer is 120 nm ± 10 nm, and corresponds to the eroded layer thickness of the rough surface morphology, measured to the base of the spikes.

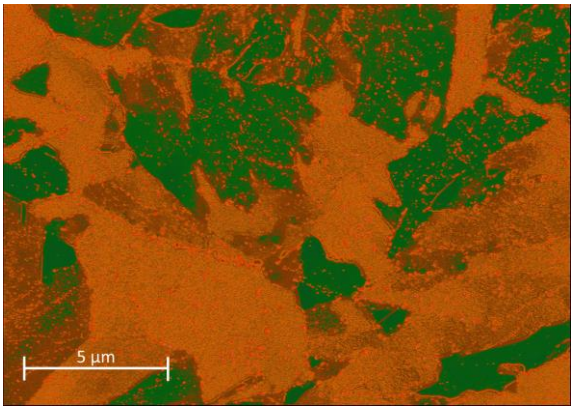

Figure 6 SEM image of spiked and smooth surface morphologies of exposed EUROFER. A contrast filter was applied to the image, marking the spiked areas in shades of orange. 70 % of the exposed surface area displays the spiked surface morphology.

Elemental depth profiles of the exposed EUROFER sample were performed by sputter-XPS. The Ar^+ beam was used to progressively erode the sample to an accumulated fluence of 3.7×10^{20} Ar m^{-2}. First, 22 measurements were taken in fluence steps of 5×10^{18} Ar m^{-2}, followed by 5 measurements in fluence steps of 5×10^{19} Ar m^{-2} to obtain W, Cr and Ta concentrations deeper into the sample. Fig. 7 shows the sputter-XPS depth profiles of W, Cr and Ta. For the analysis of the elemental composition of EUROFER, only the metallic constituents were considered (Fe, Cr, W, Ta). The concentrations of oxygen and carbon were neglected, as these were not observed in the bulk and are believed to be surface contaminants as a consequence of exposing the sample to air. W and Ta surface enrichment was confirmed, with measured concentrations peaking at the surface at roughly 16 at. % for W and 4.5 at. % for Ta. Cr is depleted at the surface because of its high sputter yield (compared with that of W and Ta), thereby contributing to the W and Ta surface enrichment. Dashed lines indicating the W and Cr depth profiles of unexposed EUROFER are included for comparison [9]. In the unexposed EUROFER, Cr is enriched near the surface due to the formation of a Cr-rich passive oxide/hydroxide layer when EUROFER is exposed to air. Such passive films typically have a thickness in the nm-range and are responsible for a high corrosion resistance in Fe-Cr and Fe-Cr-Ni stainless steels (see [26] and references therein). This Cr enrichment is less pronounced in the EUROFER sample bombarded with D because the oxide/hydroxide layer was sputtered away and Cr was depleted near the surface due to sputtering. The top x-axis indicates the approximate depth at which the given W, Ta and Cr concentrations are found, and was calculated from the sputter yield of 10 keV Ar^+ on Fe from SDTrimSP simulations (SY= 4.4 atoms per ion).

It must be noted that the concentrations shown in Fig. 7 are averaged over the XPS information depth of approximately 4 nm. Furthermore, as the Ar beam sputters the surface of the sample, the sample composition is modified by preferential sputtering, thereby compromising the sputter-XPS measurement. In order to mitigate these issues, the forward modelling code described in [24] was used in combination with SDTrimSP simulations of 10 keV Ar^+ bombardment of Fe/W/Ta mixed materials. With this method, the elemental concentrations that should be obtained through XPS were calculated at each simulated Ar^+ fluence step, taking into account effects such as preferential sputtering and ion mixing, as well as relative XPS sensitivity factors. These concentrations were compared to the measured XPS data and the process was iteratively repeated to improve the initial guesses of the Fe, W and Ta concentration profiles, until the simulated XPS spectra agreed with the measured XPS data. At this point, the resulting depth profiles represent the most likely actual concentrations of Fe, W and Ta as a function of depth, peaking at approximately 20 at. % W and 10 at. % Ta at the surface. The XPS measurements of the W concentration, the W depth profile obtained via forward modeling and the W depth profile as measured with RBS are shown in Fig. 8. If the W depth profile obtained from forward modeling is averaged over the RBS depth resolution (green dashed line in Fig. 8), it can be seen that there is good agreement between the modeled profile and the RBS data.

The uncertainty in the concentration of W and of Ta in the sputter-XPS measurements is estimated to be around 1.5 at. %. To assess the influence of the measured W and Ta enrichment on the experimental results for D sputtering, static 1-D SDTrimSP simulations were performed with the Fe, W and Ta depth profiles obtained via forward modeling [24]. The sputter yield of these simulations was compared with that of simulations without the enriched W and Ta layers, i.e., with bulk concentrations. Simulations were performed with increased and decreased W and Ta concentrations to account for the uncertainty in the XPS measurement. The inclusion of the W- and Ta-enriched surface layers is responsible for a reduction of the sputter yield of 53 % ± 3 %, i.e.,

$$SY_{Enrichment} = (1 - 0.53 \pm 0.03) \times SY_{1D\ flat} = (0.47 \pm 0.03) \times SY_{1D\ flat}.$$

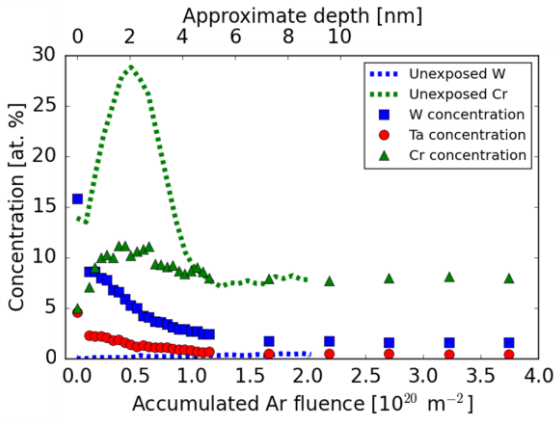

Figure 7 Elemental depth profile obtained by sputter-XPS of EUROFER with 10 keV Ar^+ after bombardment with 200 eV D to a fluence of 1.14×10^{24} D m^{-2}. Solid symbols: the elemental concentration of W, Ta and Cr are plotted as a function of the accumulated Ar^+ fluence to which the surface was sputtered. The dotted lines indicate the concentrations of W and Cr in unexposed EUROFER [9]. For the calculation of the elemental concentration, oxygen and carbon were neglected. A second x-axis is included (on top) to illustrate the approximate depth (estimated based on the sputter yield for 10 keV Ar).

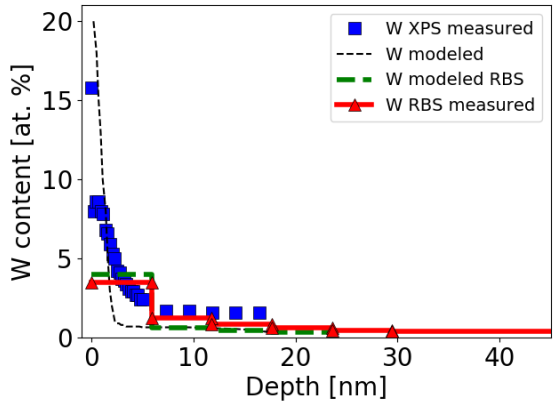

Figure 8 W elemental depth profile of EUROFER after exposure to a 200 eV D beam to a fluence of 1.14×10^{24} D m^{-2}, as measured by XPS (blue squares) and RBS (red triangles). The dashed black line represents the W concentration obtained from the XPS data with the forward modeling tool described in [24]. The dashed green line represents the same W profile averaged over the depth resolution of the RBS measurements.

The approach taken in this work, namely, assessing the effects on the sputter yield of surface morphology and of surface enrichment independently, assumes that the two variables (morphology and surface enrichment) are independent of one another, i.e., that the W concentration is similar in all areas of the sample. To check this, EDX scans were performed before and after erosion on areas featuring both kinds of surface morphologies after exposure (prior to exposure, all areas were smooth). The EDX spectra performed on the same areas of the sample before and after bombardment at SIESTA indicate a significant increase in the overall W near-surface content after exposure, qualitatively confirming the W enrichment measured by sputter-XPS. However, only slight variations

in the W or Ta concentration between each kind of morphology are observed within the measurement uncertainty of EDX before or after exposure (typically below 25 % relative difference), as exemplified in Fig. 9 for W after exposure. Therefore, the proposed assumption is not invalidated by the EDX data. It is worth noting that, under these experimental conditions, the concentration of W quantified by EDX corresponds to an interaction depth up to the range of 50 nm. Furthermore, quantification of EDX spectra may be compromised due to the presence of impurities such as C and Si. As mentioned at the beginning of this section, abundant segregations were observed in the SEM images (e.g., Fig. 3). These consist mainly of carbides with high concentrations (relative to bulk EUROFER composition) of W, Ta or other alloying elements, as evidenced by EDX (Fig. 9 for W).

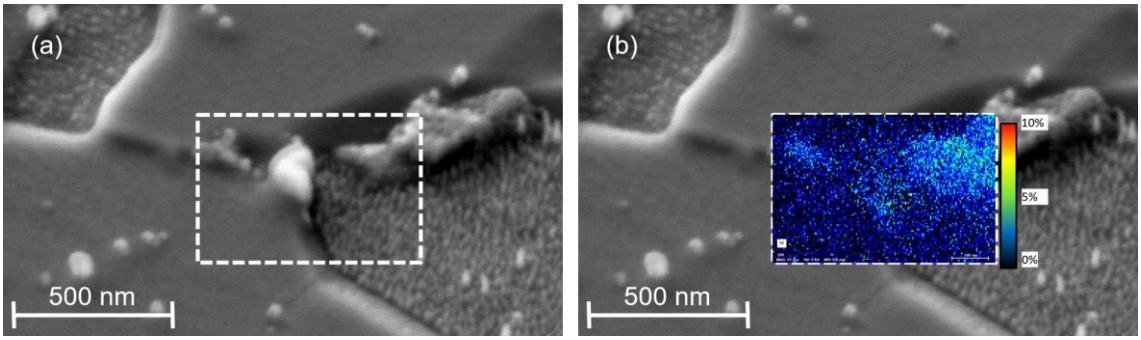

Figure 9 (a) 45°-Tilted SEM image showing spiked and smooth surface regions of exposed EUROFER. (b) EDX map displaying the distribution of W within the white dashed rectangle in the left image, with a gradient indicating the approximate relative amount of W extracted from the EDX data. The spiked and smooth surface morphologies have roughly the same W content, with a relative difference below 25 %. The bright structures in the middle, top right and top left of the white dashed rectangle in the SEM image are carbides. These carbides often have a higher W content than the areas exhibiting smooth or rough surface morphologies.

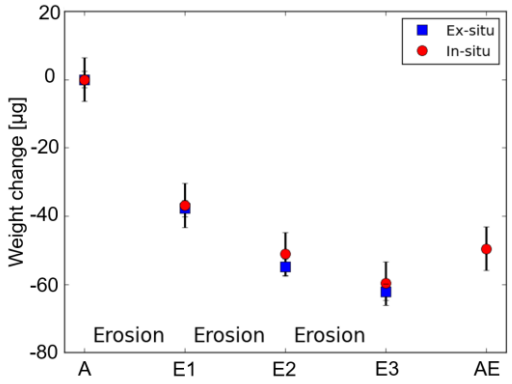

Figure 10 Ex- and in-situ weight-loss measurements of EUROFER. The weight change is plotted relative to the measured weight of the sample plus sample holder after degassing (labeled A), which is set to 0. The points on the x-axis correspond to successive weight measurements performed between exposures (E1, E2, E3), and after exposure to air (AE).

Figure 10 shows the data of the ex-situ and in-situ weight change measurements that were described in Sec. 2. The ex-situ and in-situ weight measurements of the sample with sample holder after degassing are plotted at the origin (0 µg), labeled A. All other ex-situ and in-situ weight measurements are plotted relative to the respective ex-situ and in-situ measurement after degassing. As shown in the figure, the weight of the sample decreases after each erosion step (A-E1, E1-E2, E2-E3). After step E3, the sample was demounted, stored in a desiccator, and the sample holder was exposed to air for a period of days, after which the sample was remounted on the sample holder and weighed in-situ (AE). As a consequence of its exposure to air, an increase in weight of approximately 10 µg was observed. The ex-situ weight-loss measurements seem to be lower than the in-situ measurements for the three erosion steps. However, we cannot conclusively state that the ex-situ weight loss measurements are lower, since the in-situ and ex-situ measurements agree within the experimental uncertainty.

The ex-situ and in-situ weight-loss measurements between each fluence step were used to calculate the sputter yield by applying:

$SY = \frac{\Delta mass[\mathrm{g}] \times N_A[\frac{\mathrm{atoms}}{\mathrm{mol}}]}{N_{ions} \times M\left[\frac{\mathrm{g}}{\mathrm{mol}}\right]}$, where $\Delta mass$ is the mass loss due to erosion, N_A is Avogadro's number, M is the molar mass of the target (here assumed as pure Fe), and $N_{ions} = 3 \times Q[\mathrm{C}]/e[\mathrm{C}]$ is the total amount of impinging particles (3 deuterons per impinging D_3^+ ion). Q is the collected charge at the target and e is the elementary charge.

The resulting sputter yields are listed with their standard deviations in Table 1. Sputter yields from [9] are included for comparison. Since the sputter yield is calculated from the difference of the weight measurements before and after each fluence step, the sputter yields listed here represent the average sputter yield at a fluence between the initial and final fluence, labeled "Fluence mid-point" in Tab. 1. The sputter yields from literature and the experimentally determined ex- and in-situ sputter yields show good agreement in all cases within the given ranges of uncertainty. The calculation of the uncertainty of the sputter yield considers the uncertainty in the weight-loss measurements and the uncertainty in the current measurement in SIESTA. Assuming the sputter yield of pristine EUROFER to be 0.0237, based on the empirical fit given in [9], the in-situ weight-loss measurements result in a reduction of the sputter yield from 0.0237 to 0.0068 ± 0.0012 at an equivalent fluence of 10^{24} D m^{-2}, i.e., a reduction of 71% ± 5%.

Table 1 Sputter yield of EUROFER bombarded at 300 K by 200 eV D ions (600 eV/D_3^+) to an accumulated fluence of 1.14×10^{24} D m^{-2}, determined via ex-situ and in-situ weight-loss measurements. Literature values from [9] are included for reference. Fluence mid-point indicates the intermediate fluence in that fluence step.

	Ex-situ	In-situ	Literature [9]	Fluence [10^{24} D m^{-2}]	
Erosion Step	Sputter yield	Sputter yield	Sputter yield	Mid-point	Final
A to E1	0.0164 ± 0.0030	0.0160 ± 0.0039	0.012 ± 0.0009	0.24	0.48
E1 to E2	0.0088 ± 0.0009	0.0074 ± 0.0017	0.0086 ± 0.0019	0.68	0.88
E2 to E3	0.0059 ± 0.0005	0.0068 ± 0.0012	0.0074 ± 0.0009	1.01	1.14

This measured reduction in the sputter yield can be compared to the expected reduction due to the combination of surface morphology and W & Ta surface enrichment, which is estimated as:

$$SY_{Combined} = \frac{SY_{Morphology}}{SY_{1D\ flat}} \times \frac{SY_{Enrichment}}{SY_{1D flat}} \times SY_{1D\ flat}.$$

This value is:

$$SY_{Combined} = (0.58 \pm 0.05 \times 0.47 \pm 0.03) \times SY_{1D\ flat} = (0.27 \pm 0.04) \times SY_{1D\ flat},$$

i.e., a reduction of the sputter yield of 73 % ± 4 %, which is in good agreement with the ex- and in-situ weight-loss measurements, as well as the data from [9]. It must be noted that, while the data for the modeling of the surface morphology (SEM imaging) and W & Ta surface enrichment (sputter-XPS depth profiling) correspond to EUROFER exposed to a fluence of 1.14×10^{24} D m^{-2}, the weight-loss measurements are used to calculate a sputter yield averaged between a fluence of 0.88×10^{24} D m^{-2} and 1.14×10^{24} D m^{-2}. The real sputter yield at a fluence of 1.14×10^{24} D m^{-2} may in fact be lower than the values listed in Table 1, therefore leading to an even stronger reduction of the sputter yield. However, as shown in [9], the change in the sputter yield between accumulated fluences of 0.88×10^{24} D m^{-2} and 1.14×10^{24} D m^{-2} should be very small, and can be assumed to lie within the experimental uncertainty given in the weight-loss measurements. Table 2 lists the expected reduction in the sputter yield of EUROFER due to surface morphology and W & Ta surface enrichment at the final accumulated fluence, in comparison with the measured values.

Table 2 Reduction of the sputter yield of EUROFER bombarded with 200 eV deuterium to an equivalent fluence of 10^{24} D m^{-2} due to surface morphology and surface enrichment of W and Ta, compared with the sputter yield reduction measured experimentally by weight-loss (ex-situ and in-situ) and from literature [9].

		Fraction of $SY_{SDTrimSP}$	Reduction of
Modeled factors	Surface morphology	0.58 ± 0.054	42 % ± 5 %
	Surface enrichment	0.47 ± 0.03	53 % ± 3 %
	Total	0.27 ± 0.04	73 % ± 4 %
Weight-loss	Ex-situ	0.25 ± 0.02	75 % ± 2 %
	In-situ	0.29 ± 0.05	71 % ± 5 %
	Literature [9]	0.31 ± 0.04	69 % ± 4 %

It can be concluded that both surface morphology and surface enrichment play a major role in the sputtering behavior of EUROFER under bombardment with 200 eV deuterium. Only their combined effect can explain the reduction in the sputter yield observed experimentally and in the literature. However, it must be noted that no experimental data is available for the initial sputter yield of pristine EUROFER. The value used here to normalize the experimentally determined sputter yields is based on an empirical fit to experimental data from [9] obtained at higher fluences, and as such is subject to uncertainty. No quantification of this uncertainty is given in [9].

As already mentioned at the beginning of this section, open questions remain in the analysis of the surface morphologies present in exposed EUROFER. The development of cone- or pyramid-like structures during ion bombardment has been observed in the past [27,28,29,30]. In these studies, the growth of these structures was modeled by a stress-induced growth mechanism and the nucleation of these features was associated with impurities or defects, such as dislocations. The process for the nucleation of these structures, in particular the presence of impurities, may in some cases also apply for the spikes shown in this work. As is discussed in the following section, dynamic 3-D simulations of FeW with 2 at.% W bombarded with D show that W tends to cluster on the surface, forming the tip of a spike as the surrounded area is preferentially eroded. However, marked discrepancies exist between the cones seen in the literature and the spikes shown here. The cones have a typical height and width in the µm range, i.e. are roughly 2 orders of magnitude larger than the spikes shown in this work. Furthermore, in [27,28] the cones are shown to be faceted, which could indicate a preferential orientation of the sides of the cones along the crystal lattice. No such faceting is observed in this work. Therefore, it cannot presently be concluded that the growth of the spikes studied in this work (or their lack of growth in the smooth surfaced-areas) is governed by a similar stress-induced mechanism.

As is shown in Sec. 2, bombardment of mirror-polished EUROFER leads to the formation of two distinct morphologies for the exposure conditions investigated here (200 eV D, about 300 K sample temperature), one smooth and one spiked, with the former being more resistant to sputtering than the latter. It is presently unknown why these two morphologies develop and why they exhibit such a strong difference in their sputtering behavior. This effect cannot be due to the initial surface roughness as prior to sputtering AFM scans and SEM images revealed that all areas on the sample were smooth. Furthermore, as evidenced by the SDTrimSP-3D calculations, the spiked geometry that develops during exposure should lead to reduced sputtering compared with a smooth surface. Therefore, the cause for this difference in the sputtering behavior must be some other factor, such as grain-orientation dependence [31] or inhomogeneous material composition. The following section describes additional investigations performed on the EUROFER samples investigated in this work and possible avenues for further research.

4 Effect of grain orientation and W-clustering

EBSD was performed prior to exposure at pre-defined positions. One such position is shown in Figure 11. An SEM image of exposed EUROFER is displayed alongside an EBSD image of the same area. In

the SEM image, darker gray areas correspond to a smooth surface morphology, while lighter gray areas feature a rough surface morphology. The grains are visible in the EBSD image and have been color coded according to the grain orientation given by their Miller indices in the direction normal to the surface. By comparing enlarged views of the images (not shown), it can be seen that boundaries between the two surface morphologies (visible as darker and lighter areas in the SEM image) coincide with grain boundaries. That is to say, within the same grain, only one type of surface morphology is present, either smooth or spiked. Therefore, it is assumed that the difference in sputtering behavior between the two kinds of surface morphologies can be ascribed to differences between the grains themselves. One possibility would be that grains that exhibit different surface morphologies also exhibit different metallurgic phases: ferrite, martensite or retained austenite. However, EBSD imaging classified all grains as corresponding to a bcc lattice, i.e., no austenite was present. Furthermore, EUROFER is designed to be fully martensitic (ferrite content << 30%), as mentioned in [2] and observed experimentally in [32,33,34]. Therefore, the differences in sputtering behavior cannot be explained by differences in the metallurgic phase.

Another possible cause for the observed differences would be grain orientation. A systematic analysis of this hypothesis was performed by automatically associating grain orientations to height information from CLSM data. Such an analysis is described in more detail for W in [22]. As shown in Fig. 12, this analysis indicates that some grain orientations are indeed eroded more than others are. Since areas with a larger eroded layer thickness correspond to areas with a spiked morphology (Fig. 3), there exists a correlation between grain orientation and the surface morphology of a given grain.

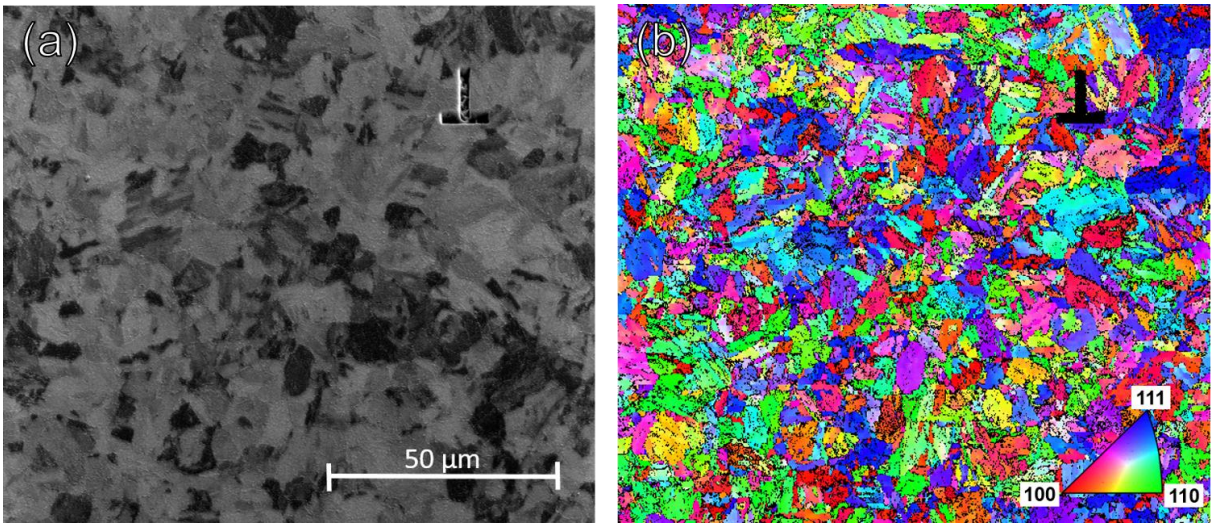

Figure 11 (a) SEM image of exposed EUROFER. The rotated T-shaped FIB marker is visible in the upper right quadrant. Areas with a smooth surface morphology appear darker in the SEM image. (b) EBSD image of the same area, indicating the grain orientation. The FIB marker appears as a black area. The grains are color-coded according to their orientation in the direction normal to the surface, as given by the inverse pole figure in the lower right corner. The Miller indices 100, 111 and 110 correspond to red, blue and green, respectively.

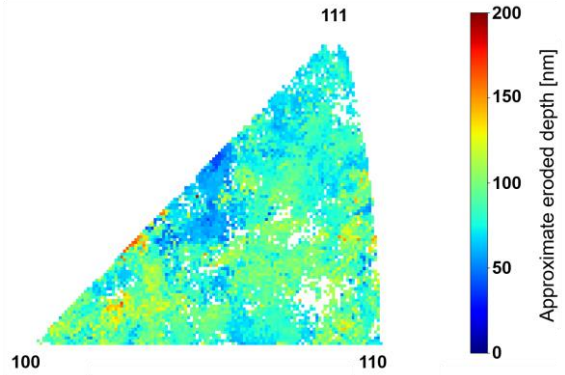

Figure 12 Inverse pole plot obtained from a combined evaluation of EBSD (Fig. 10) and CLSM data after erosion, showing the approximate eroded depth as a function of grain orientation in the direction normal to the sample surface. Though there seems to be a correlation between grain orientation and eroded depth (neighboring areas of the plot at the pixel length-scale tend to have similar color), the nature of this relationship is not evident from the plot.

The different sputtering behavior observed for the smooth and spiked surface morphologies could also be a consequence of differences in the composition of the grains. No substantial differences were observed in EDX spectra of the W or Ta surface concentrations, which could directly influence the sputter yield of the mixed material. However, it should be noted that, given the interaction volume of EDX of approximately 50 nm, small differences in the concentrations of these elements within the top surface layers would be difficult to detect with EDX.

A possible explanation that would be consistent with the EDX and EBSD data could involve clustering of W atoms in the near-surface region of EUROFER. Dynamic SDTrimSP-3D simulations [20] of 200 eV D bombardment of FeW with 2 at. % W were performed here. In these simulations, due to preferential sputtering of Fe and ion mixing, W tends to progressively cluster, protecting the area underneath. This has the effect of leading to the formation of a spiked surface morphology like the one observed in SEM images. If the 2 at. % W is distributed homogeneously in the target, a larger fluence is required to achieve the same spiked surface morphology than if the 2 at. % W is distributed inhomogeneously (already presents some degree of clustering prior to sputtering), i.e., if W is distributed homogeneously, the surface remains smooth for longer. Figure 13 shows simulations with homogeneous targets and with initially inhomogeneous targets (W clustered into cells of $1\times1\times1$ nm^3 or $5\times5\times5$ nm^3), bombarded by 200 eV D to varying fluences. The cell size in all simulations was $0.5\times0.5\times0.5$ nm^3, with a simulated surface area of 100×100 nm^2. Since in the simulations the 2% of W atoms are mostly surrounded by Fe, the displacement energy of both the Fe and W atoms was set to 17 eV, i.e. the displacement energy of an atom in a pure Fe matrix. 10000 fluence steps were performed for each simulation, with 40000 particles simulated per fluence step.

If different grains present a different profile of W-distribution, for example due to different grain orientation, then it is conceivable that some grains would lead to the formation of spiked surface morphologies before others. Furthermore, in the simulations with 2% W distributed homogeneously the sputter yield is lower than in the simulations where the 2% W is clustered, which contributes to the surface remaining smooth at higher fluences. This is qualitatively in agreement with the experimental observations, which show that the smooth surfaces have been eroded less than the areas exhibiting a spiked morphology. Under this hypothesis, the fraction of the surface that is smooth or spiked should be a function of the impinging ion fluence. It is possible that, at this fluence, grains with more pronounced W-clustering have already developed such a morphology, while grains with W more homogeneously distributed will only do so at higher fluences. This will be tested in experiments involving the bombardment of EUROFER to fluences of several 10^{24} D m^{-2}, as was done in [9, 35].

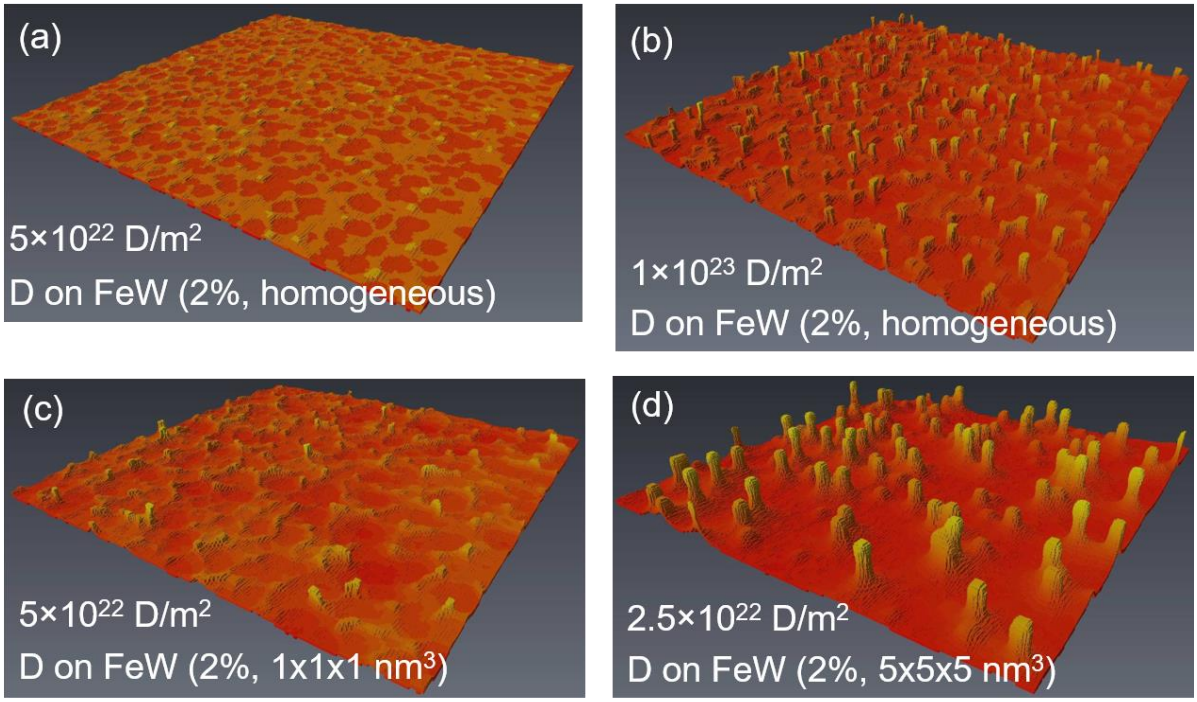

Figure 13 Dynamic SDTrimSP-3D simulations of FeW with 2 at. % W distributed either homogeneously (a & b) or clustered into cells of 1×1×1 nm^3 (c) or 5×5×5 nm^3 (d). The targets were bombarded with 200 eV D to varying fluences. In all cases, a spiked surface morphology develops, similar to the one observed in SEM images (Fig. 2). The fluence required for the development of this morphology is dependent on the initial degree of W clustering. The simulated surface area is in all cases 100×100 nm^2. The length scale in the direction normal to the surface is the same as in the directions parallel to the surface.

5 Summary

In this work, the surface morphology and composition of EUROFER were characterized before and after exposure to 200 eV D to a fluence of 1.14×10^{24} D m^{-2} at 300 K. The goal of these experiments was to assess the impact of the surface morphology and of the W and Ta surface enrichment on the sputter yield. The former was determined with the aid of SEM imaging and SDTrimSP-3D simulations. For the latter, sputter-XPS depth-profiling and static 1-D calculations with SDTrimSP were employed, coupled with RBS depth-profiling. The combined effect of these factors was compared with sputter yields determined experimentally via weight-loss measurements and with data from the literature. SEM imaging after ion bombardment revealed two distinct surface morphologies, consisting of smooth areas and areas displaying a spiked morphology (shown in Fig. 2). EDX was employed to verify that the W content in the two surface morphologies is similar within the measurement uncertainty (Fig. 9). The size of these spikes was extracted from the SEM images and was used to construct a 3-D model of the surface for SDTrimSP-3D simulations (Fig. 4). According to these simulations, the spiked surface geometry is responsible for a 24 % decrease in the sputter yield compared with a perfectly smooth surface. It was observed that the smooth areas were eroded substantially less than the spiked areas (Fig. 3), corresponding to a sputter yield between zero (no erosion, surface stays smooth) and 30 % of the value calculated with SDTrimSP. Approximately 70 % of the surface of the sample features the spiked morphology (Fig. 6), while the remaining 30 % remain smooth. The overall effect of surface morphology on the sputtering of EUROFER under these conditions is a reduction in the sputter yield of 42 % ± 5 %.

Depth profiles performed by sputter-XPS were evaluated with a forward modelling code that corrected for ion mixing, preferential sputtering and XPS sensitivity. Surface enrichment of W and of Ta were confirmed, with concentrations of W at the surface of 20 at. %, as shown in Fig. 8, i.e., enriched by more than a factor of 60. Static SDTrimSP simulations employing the experimentally-obtained W and Ta depth profiles revealed a reduction of the sputter yield of 53 % ± 3 % when compared with

simulations with a homogeneous W and Ta distribution corresponding to bulk EUROFER. The combined effects of surface morphology and W & Ta enrichment on the sputtering behavior of EUROFER under these conditions are therefore estimated to be responsible for a reduction in the sputter yield of 73 % ± 4 %. This value is compared with a measured reduction in the sputter yield from 0.0237 (initial value based on the empirical fit from [9]) to 0.0068 ± 0.0012 (determined by in-situ weight-loss at an equivalent fluence of 1×10^{24} D m^{-2}), i.e., a reduction of 71 % ± 5 %. Both surface morphology and surface enrichment contribute significantly to the reduction of the sputter yield of EUROFER under the given experimental conditions, and only their combined effect is sufficient to explain the reduction in the sputter yield observed in weight-loss experiments and in the literature (Tab. 2).

The existence of a heterogeneous surface morphology with different sputtering behavior within EUROFER has hitherto not been taken into account in simulations with tools such as SDTrimSP. The methodology shown here constitutes the first approach to consider the effect of surface morphology on the sputter yield of EUROFER and provides a better quantitative agreement with the experimental data than other works from literature that only considered W surface enrichment [9]. In addition, the correlation between grain orientation, surface morphology and erosion behavior was investigated and a possible explanation involving W-clustering was discussed. However, it should be noted that this experiment comprises only one exposure scenario and hinges on several assumptions that could not be proved or disproved, such as the lateral homogeneity of the W concentration on the nm-scale. It can be anticipated that further research on the origin and evolution of these surface morphologies may allow for better understanding of the sputtering evolution of EUROFER. This would further enable better predictions of the sputter yield of EUROFER under reactor-relevant exposure conditions.

Acknowledgements

This work has been carried out within the framework of the EUROfusion Consortium and has received funding from the Euratom research and training programme 2014-2018 and 2019-2020 under grant agreement No 633053. The views and opinions expressed herein do not necessarily reflect those of the European Commission. Work performed under EUROfusion WP PFC.

References

[1] R. Lindau et al., “Present development status of EUROFER and ODS-EUROFER for application in blanket concepts”, Fusion Eng. Des., vol. 75-79, 989–996, 2005.

[2] B. van der Schaaf et al., “The development of EUROFER reduced activation steel”, Fusion Eng. Des. 69, 197, 2003.

[3] V. Chernov et al., “Structural materials for fusion power reactors - the RF R&D activities”, Nuclear Fusion, vol. 47, 8, 839, 2007.

[4] S. Jitsukawa et al., “Development of an extensive database of mechanical and physical properties for reduced-activation martensitic steel F82H”, J. Nucl. Mater. 307–311, 179–186, 2002.

[5] Q. Huang et al., “Development status of CLAM steel for fusion application”, J. Nucl. Mater. 455, 649–654, 2004.

[6] G. Federici et al., “Assessment of erosion and tritium codeposition in ITER-FEAT”, J. Nucl. Mater., vol. 290-293, 260 – 265, 2001.

[7] R. Behrisch et al., “Material erosion at the vessel walls of future fusion devices”, J. Nucl. Mater., 313-316, 2003.

[8] R. Arredondo, *SIESTA: A new ion source setup and its application to erosion studies on first-wall materials for fusion reactors*, PhD thesis, Technische Universität München, 2019.

[9] K. Sugiyama et al., “Erosion of EUROFER steel by mass-selected deuterium ion bombardment”, Nuclear Materials and Energy, vol. 16, 114 – 122, 2018.

[10] P. Ström et al., “Compositional and morphological analysis of FeW films modified by sputtering and heating”, Nuclear Materials and Energy, vol. 12, 472 – 477, 2017.

[11] P. Ström et al., “Sputtering of polished EUROFER97 steel: Surface structure modification and enrichment with tungsten and tantalum”, Journal of Nuclear Materials, vol. 508, 139 – 146, 2018.

[12] M. Balden et al., “Effect of the surface temperature on surface morphology, deuterium retention and erosion of EUROFER steel exposed to low-energy, high-flux deuterium plasma”, Nuclear Materials and Energy, vol. 12, 289 – 296, 2017.

[13] R. Koslowski et al., “Temperature-dependent in-situ LEIS measurement of W surface enrichment by 250 eV D sputtering of EUROFER”, Nuclear Materials and Energy, vol. 16, 181, 2018.

[14] Y. Martynova et al., “Deuterium retention in RAFM steels after high fluence plasma exposure”, Nuclear Materials and Energy, vol. 12, 648-654, 2017.

[15] V. Alimov et al., “Surface modification and deuterium retention in reduced-activation steels exposed to low-energy, high-flux pure and helium-seeded deuterium plasmas”, Journal of Nuclear Materials, vol. 502, 1 – 108, 2018.

[16] J. Roth et al., “EUROFER as wall material: Reduced sputtering yields due to W surface enrichment”, Journal of Nuclear Materials, vol. 454, 1, 2014.

[17] A. Mutzke et al., *SDTrimSP Version 6.00*. IPP Report 2019-02, Max-Planck-Institut für Plasmaphysik (Ed.) http://hdl.handle.net/21.11116/0000-0002-F6AE-5, 2019.

[18] W.Eckstein, *Computer Simulation of Ion-Solid Interactions*. Springer Berlin Heidelberg, 1991.

[19] R. Arredondo et al., “SIESTA: a high current ion source for erosion and retention studies”, Rev. Sci. Instrum., vol. 89, 103501, 2018.

[20] U. von Toussaint et al., “Sputtering of rough surfaces: a 3D simulation study”, Phys. Scr., vol. 2017, T170, 014056, 2017.

[21] R. Arredondo et al., “Angle-dependent sputter yield measurements of keV D ions on W and Fe and comparison with SDTrimSP and SDTrimSP-3D”, Nucl. Mater. Energy, vol. 18, 72–76, 2019.

[22] K. Schlueter et al., “Dependence of oxidation on the surface orientation of tungsten grains”, International Journal of Refractory Metals and Hard Materials, vol. 79, 102–107, 2019.

[23] K. Sugiyama et al., “Sputtering of iron, chromium and tungsten by energetic deuterium ion bombardment”, Nucl. Mater. Energy, vol. 8, 1–7, 2016.

[24] G. Meisl et al., “Implantation and erosion of nitrogen in tungsten”, New J. Phys., vol. 16, 093018, 2014.

[25] M. Mayer. *SIMNRA User’s Guide*. Tech. rep. IPP 9/113. Garching: Max-Planck-Institut für Plasmaphysik, 1997.

[26] Z. Wang et al., “Mechanisms of Cr and Mo Enrichments in the Passive Oxide Film on 316L Austenitic Stainless Steel”, Frontiers in Materials, vol. 6, 232, 2019.

[27] J.L. Whitton et al., “The development of cones and associated features on ion bombarded copper”, Radiation Effects, 32:3-4, 129-133, 1977.

[28] S.M. Rossnagel et al., “Impact enhanced surface diffusion during impurity induced sputter cone formation”, Surface Science, vol. 123:1, 89-98, 1982.

[29] A.K. Sen et al., “Surface topography of eroded Cu and Si cathodes in a PIG ion source”, Bull. Mater. Sci., vol 16:3, 193-204, 1993.

[30] L.B. Begrambekov et al., “Peculiarities and mechanism of the cone growth under ion bombardment”, Materials and Atoms, vol.115:1-4, 456-460, 1996.

[31] H.E. Roosendaal, *Sputtering Yields of Single Crystalline Targets*, Ch. 5 in *Sputtering by Particle Bombardment I*, R. Behrisch (Ed.), Springer Berlin Heidelberg, 1981.

[32] K. Mergia et al., “Structural, thermal, electrical and magnetic properties of Eurofer 97 steel”, Journal of Nuclear Materials, vol.373, 1-8, 2008.

[33] Z. Lu et al., “Effect of heat treatment on microstructure and hardness of Eurofer 97, Eurofer ODS and T92 steels”, 386-388, 445-448, 2009.

[34] P. Fernández et al., “Metallurgical characterization of the reduced activation ferritic/martensitic steel Eurofer’97 on as-received condition”, Fusion Engineering and Design, 58-59, 787-792, 2001.

[35] O.V. Ogorodnikova et al., “Surface modification and deuterium retention in reduced-activation steels under low-energy deuterium plasma exposure. Part I: undamaged steels”, Nucl. Fusion, vol. 57, 2016.